Available online at www.sciencedirect.com

ScienceDirect

Journal of the Franklin Institute 353 (2016) 4715–4733

Journal of The Franklin Institute

www.elsevier.com/locate/jfranklin

Blind image quality assessment for Gaussian blur images using exact Zernike moments and gradient magnitude

Chern-Loon Lim[a], Raveendran Paramesran[a,*], Wissam A. Jassim[a], Yong-Poh Yu[b], King Ngi Ngan[c]

[a]Department of Electrical Engineering, Faculty of Engineering, University of Malaya, Lembah Pantai, 50603 Kuala Lumpur, Malaysia

[b]Department of Science and Engineering, Center for Foundation Studies, Universiti Tunku Abdul Rahman, 43000 Kajang, Selangor, Malaysia

[c]Department of Electronic Engineering, The Chinese University of Hong Kong, Shatin, Hong Kong

Received 4 April 2016; received in revised form 22 July 2016; accepted 13 August 2016
Available online 1 September 2016

Abstract

Features that exhibit human perception on the effect of blurring on digital images are useful in constructing a blur image quality metric. In this paper, we show some of the exact Zernike moments (EZMs) that closely model the human quality scores for images of varying degrees of blurriness can be used to measure these distortions. A theoretical framework is developed to identify these EZMs. Together with the selected EZMs, the gradient magnitude (GM), which measures the contrast information, is used as a weight in the formulation of the proposed blur metric. The design of the proposed metric consists of two stages. In the first stage, the EZM differences and the GM dissimilarities between the edge points of the test image and the same re-blurred image are extracted. Next, the mean of the weighted EZM features are then pooled to produce a quality score using support vector machine regressor (SVR). We compare the performance of the proposed blur metric with other state-of-the-art full-reference (FR) and no-reference (NR) blur metrics on three benchmark databases. The results using Pearson's correlation coefficient (CC) and Spearman's ranked-order correlation coefficient (SROCC) for the LIVE image database are 0.9659 and 0.9625 respectively. Similarly, high correlations with the subjective scores are achieved for the other two databases as well.

*Corresponding author.
E-mail addresses: limchernloon@gmail.com (C.-L. Lim), ravee@um.edu.my (R. Paramesran), binaye2001@yahoo.com (W.A. Jassim), richieyyp@yahoo.com (Y.-P. Yu), knngan@ee.cuhk.edu.hk (K.N. Ngan).

http://dx.doi.org/10.1016/j.jfranklin.2016.08.012
0016-0032/

1. Introduction

With the increasing popularity of digital cameras and the internet in the 21st century, digital images play an important role in human life. They are stored in the computer, posted online in such websites as Facebook, Flickr and Instagram, displayed on digital frames or burnt into digital media such as the digital versatile disc (DVD) and the compact disc (CD). However, digital photos taken from cameras maybe have various distortion types. One of them is blur, which includes the motion blur (due to camera movement or camera shake, object movement and slow shutter speed), and the out-of-focused blur (incorrect camera auto-focusing or focusing at the wrong subject of interest). Efficient image quality assessment algorithms, therefore, are essential for the selection of the digital images for final production in photo-books, posters and magazines to ensure that they are above the minimum quality level.

Image quality assessment (IQA), at least to some extent, is still based on human observers' opinions. Human beings are the ultimate receivers in most image processing environments, so they are the final image quality assessors. Based on the characteristics of the human visual system (HVS), subjective metrics, such as Mean Opinion Scores (MOS) and Difference Mean Opinion Scores (DMOS) have been developed to measure perceptual quality. However, it is not desirable to incorporate human assessment into a real-time system because it is time-consuming for human to evaluate each and every image, and it is costly to hire man power to do so. Thus, various methods have been proposed to evaluate the image quality objectively to be in line with the subjective human evaluation. IQA can be divided into three categories: *full-reference* (FR), *reduced-reference* (RR) and *no-reference* (NR) [43,23]. Without a comparison target, typically it is more difficult to develop a NR image quality metric (IQM). Thus, many researchers have been attracted to meet the challenges involved in developing better NR IQM approaches and features [24,7,26].

One issue that has challenged researchers in image processing field is the relevance of extracting features for image analysis. One of the widely used features is moments. Since the introduction of geometric moments by Hu in 1962 [17], various moments have been proposed. Some of the widely used moments are Legendre moments [38], Zernike moments [38], Tchebichef moments [28] and Krawtchouk moments [50]. Except for geometric moments, they are orthogonal and good signal descriptors. Thus, they have been used in a wide array of applications, including object classification [10], biometric [1], biomedical imaging [18,22], content-based retrieval [31,48,30], edge detection [16], focus measure [49] and recently, image quality assessment [46,40].

One particular moment that interests us is Zernike moments (ZMs). One of their inherent properties is that they are rotation invariant and robust to noise [39]. However, the computation of ZMs introduces numerical errors. Exact Zernike moments (EZMs), which retain all the advantages of ZMs, was introduced to eliminate the numerical errors [45,21].

An important characteristic in choosing NR IQA features to estimate the degree of blurriness is that they should closely exhibit human visual system (HVS) perception of image blur distortion. For the same degree of blurriness on any direction of the edges, the chosen features should ideally remain the same. Since EZMs are rotationally invariant, they can be considered to be used as edge descriptors. In this paper, we derive a set of EZMs that closely exhibit human quality score for images of various degrees of blurriness. Inspired by these advantages, a no-reference blur metric is formulated using the proposed EZMs and gradient magnitude (GM) which acts as a weight to encode the contrast information. A total of six EZMs are used in this study. The mean product of the EZMs differences and GM dissimilarities of the test image and the re-blurred

version of the test image are fed to a trained support vector machine (SVM) regressor (SVR) to assign a quality score.

There are three contributions in this paper:

- We propose a no-reference blur metric using this set of EZMs together with gradient magnitude for blur image quality assessment.
- We derive a mathematical relation between the low order EZMs of the Gaussian point spread function (PSF) and the standard deviation of the Gaussian distribution.
- We use this relation and show the proposed set of EZMs for Gaussian blur image closely model the human evaluation score for digital images from LIVE image database [35] with various blur degrees.

This paper is organized as follows. An overview of existing NR IQM for blur images is given in Section 2. Section 3 provides the basic theory of EZMs and its formulation from exact geometric moment. The theoretical framework to identify the set of EZMs that closely model the HVS perception on blur images is presented in Section 4. Next, the formulation of the proposed NR blur metric based on the identified EZMs and GM is developed. In Section 5, the performance of the proposed blur metric with other state-of-the-art metrics using three databases is demonstrated. Section 6 concludes the study.

2. Overview of existing blind image quality assessment for blur images

This section presents an overview of the existing no-reference blur quantification algorithms. Blurring can be described as attenuation of high frequency information of the image and out-of-focus blur is usually modeled by the convolution of the image with a Gaussian kernel. The severity of the blurring is denoted by the standard deviation of the Gaussian distribution. The existing NR IQMs focus on the high frequency and wavelet contents, information regarding the edges and statistical approaches. We briefly describe some of the available NR IQMs in the following paragraphs.

Firestone et al. [15] proposed a frequency threshold metric that sum all the frequency component magnitudes above a threshold Ω. The metric is higher when the image is sharper. However, the problem with this metric is that it becomes more susceptible to noise when the threshold is increased. Shaked and Tastl [34] introduce a metric based on the high-pass to band-pass frequency ratio of extracted local features. The image is sharper if the ratio is higher since it has more high-frequency content.

In [24], the image is divided into 8×8 blocks. The blurriness of the image is determined by the histogram of the discrete cosine transform (DCT) coefficients. The metric is lower for sharper image. Caviedes et al. [4] compute the kurtosis of the 8×8 DCT blocks to measure their peakedness. The kurtosis measurement is for each of the 8×8 block. A global measure of the blur of the image is computed by taking the mean value of the kurtosis of all the blocks. Cosine transform coefficients based descriptors are used in BLIINDS-II [33] as well.

Ferzli and Karam [12] applied a dyadic wavelet transform at different scales to the image, to measure the sharpness of the perceptual blur metric based on the absolute values of the horizontal and vertical bands. The metric, is lower if the image is sharper. The Haar wavelet transform (HWT) is applied in [41] to quantify edge sharpness. Edge maps are constructed after performing the HWT. Thresholding is used to determine whether the image is blur. The blur extent of the image is computed from the blur confident coefficient. Again, the metric is lower for sharper

image. Shen et al. [37] proposed a hybrid no-reference (HNR) model based on curvelet, wavelet and DCT. The authors in [27] extracted local descriptors in wavelet domain for DIIVINE.

Edges provide vital information for human to subjectively quantify the sharpness of the image. Most of the NR IQM in this approach begin with edge detection. Marziliano et al. [25] measured the edge width by computing the start position and end position of the located edge through edge detection. The perceptual blur metric is computed by averaging the edge widths of the local blur values over all the found edges. Crete et al. [9] proposed a no-reference perceptual blur metric based on the discrimination between different levels of blur perceptible on the same image. In [13], Ferzli and Karam detect 64×64 blocks classified as edge blocks. Based on the estimated local contrast and edge width, block distortion is computed. The perceptual-based sharpness metric based on probability summation is computed by taking the inverse of the pooling of the block distortions. They also proposed a blur metric based on cumulative probability of blur detection [29]. They detected edges, and then estimated the probability of detecting blur at the edges. The cumulative probability of blur detection was then used to construct the blur metric.

Statistical approaches have been widely used in NR IQM as well. A blur metric based on the variance of the whole image was proposed in [11]. As the blurriness increases, the variance of the image decreases. Batten [3] proposed an auto-correlation metric based on the difference between auto-correlation values at vertical and horizontal directions. The auto-correlation values increase if the image is blur, and the sum of the difference metric decreases. Histogram has been used in [15] and [7]. Histogram threshold metric [15] is defined as the sum of histogram bins weighted by their gray-scale values above a certain threshold. The assumption made is that sharper image contains more gray scale levels. The histogram will be wider, and thus the metric is higher. Histogram entropy-based metric, proposed by Chern et al. [7], measures the information content of the image. The entropy is high if the probability of occurrence of each gray level is low. Sharper images contain a larger number of gray levels, thus, a lower probability and higher entropy. Zhang et al. [52] showed that the spectral density function can be considered as a 2-D probability density function of a bi-variate random vector. According to them, a blur image has lower kurtosis, and thus lower metric, and vice versa. Li et al. [20] measured the kurtosis difference between the image and the re-blurred version of that image. Edge detection is performed to get edge points. 5×5 block is centered at each edge point. They define sub-blocks as 'blocks enclosing an edge pixel' (BEEP). The sub-block having the largest variance is chosen to characterize the BEEP. The normalized sum of kurtosis of the selected sub-blocks is used to construct the blur index. Mittal et al. [26] modeled the normalized image pixel value using generalized Gaussian distributions (GGD), and model the product of the neighboring pixels by asymmetric generalized Gaussian distribution (AGGD) in BRISQUE. The BRISQUE score is then applied in image restoration application. Xue et al. [47] utilized the joint statistics of gradient magnitude (GM) map and Laplacian of Gaussian (LOG) responses in their BIQA model.

3. Preliminaries

3.1. Zernike Moments (ZMs)

Two dimensional ZM of order p and repetition q of an image intensity function $f(r,\theta)$ is defined as [21]:

$$Z_{p,q} = \frac{p+1}{\pi} \int_0^1 \int_0^{2\pi} V^*_{p,q}(r) f(r,\theta) r \, \mathrm{d}r \, \mathrm{d}\theta \tag{1}$$

where ✻ denotes a complex conjugate, p is a non-negative integer, q is an integer such that $p \equiv q \pmod 2$, and $|q| \le p$. The p-th order polynomial with repetition q is defined as

$$\begin{aligned} V_{p,q}(r) &= R_{p,q}(r)e^{\hat{j}q\theta} \\ &= e^{\hat{j}q\theta} \sum_{\substack{k=q \\ p \equiv k(\mathrm{mod}2)}}^{p} B_{p,q,k} r^k \end{aligned} \tag{2}$$

where $r = \sqrt{x^2 + y^2}$, $r \in [-1, 1]$ is the length of the vector from the image pixel (x,y) to the origin, $\theta =$ arctan (y/x) is the angle between vector r and the principal x-axis and $\hat{j}$ is $\sqrt{-1}$. The polynomial coefficient $B_{p,q,k}$ is generated as

$$B_{p,q,k} = \frac{(-1)^{\frac{p-k}{2}} \left(\frac{p+k}{2}\right)!}{\left(\frac{p-k}{2}\right)! \left(\frac{k+q}{2}\right)! \left(\frac{k-q}{2}\right)!} \tag{3}$$

For a two discrete image intensity function $f(x, y)$ of size $N \times N$, ZM of Eq. (1) is approximated as

$$Z_{p,q} = \frac{p+1}{\pi} \sum_{i=0}^{N-1} \sum_{j=0}^{N-1} V^*_{p,q}(x, y) f(x, y), x_i^2 + y_j^2 \le 1 \tag{4}$$

ZMs can be expressed in term of geometric moments by the following relationship:

$$Z_{p,q} = \frac{p+1}{\pi} \sum_{\substack{k=q \\ p \equiv k(\mathrm{mod}2)}}^{p} \sum_{m=0}^{s} \sum_{n=0}^{q} \left(-\hat{j}\right)^n \times \binom{s}{m} \binom{q}{n} B_{p,q,k} M_{k-2m-n,2m+n} \tag{5}$$

where $s = (k-q)/2$, $\hat{j} = \sqrt{-1}$ and $M_{p,q}$ is the discretized geometric moment given by

$$M_{p,q} = \sum_{x=0}^{N-1} \sum_{y=0}^{N-1} x^p y^q f(x, y) \tag{6}$$

3.2. Exact Zernike moments (EZMs)

The original form of $M_{p,q}$ is in continuous domain, and hence the approximation of double integrals by double summations over a fixed sampling interval in Eq. (6) introduces numerical errors. As the number of sampling points increases, the numerical errors also increase. In order to avoid the generation of these errors, exact geometric moments is computed by rewriting Eq. (6) as

$$EGM_{p,q} = \sum_{i=0}^{N-1} \sum_{j=0}^{N-1} h_{p,i} h_{q,j} f(i, j) \tag{7}$$

where $h_{p,i}$ and $h_{q,j}$ can be expressed by using the normal mathematical integration rule [45]:

$$h_{p,i} = \int_{x_i - \Delta x_i/2}^{x_i + \Delta x_i/2} x^p \mathrm{d}x = \left[\frac{x^{p+1}}{p+1}\right]_{x_i - \Delta x_i/2}^{x_i + \Delta x_i/2}$$

$$h_{q,j} = \int_{y_j - \Delta y_j/2}^{y_j + \Delta y_j/2} y^q \mathrm{d}y = \left[\frac{y^{q+1}}{q+1}\right]_{y_j - \Delta y_j/2}^{y_j + \Delta y_j/2} \tag{8}$$

EZMs can be computed by substituting Eq. (7) into Eq. (5):

$$EZM_{p,q} = \frac{p+1}{\pi} \sum_{\substack{k=q \\ p-k=even}}^{p} \sum_{m=0}^{s} \sum_{n=0}^{q} (-\hat{j})^n \times \binom{s}{m}\binom{q}{n} B_{p,q,k} EGM_{k-2m-n,2m+n} \tag{9}$$

where $B_{p,q,k}$ is calculated using Coefficient Method in [8].

3.3. Zernike moments of the blurred image

Let $g(x,y)$ be a blurred version of the original image $f(x,y)$. Under the condition that imaging system being linear shift-invariant, the blurring can be described by the convolution

$$g(x,y) = (f * h)(x,y) \tag{10}$$

where $h(x,y)$ is the PSF of the imaging system, and $*$ denotes the linear convolution. In this paper, the PSF, $h(x,y)$ is referred to the Gaussian kernel, given by

$$h(x,y) = \frac{1}{2\pi\sigma^2} \cdot e^{-\frac{x^2+y^2}{2\sigma^2}} \tag{11}$$

where the σ is the standard deviation of the Gaussian distribution. Assume that the imaging system is energy-preserving and the Gaussian kernel is a circularly symmetric function, which lead to

$$h(x,y) = h(r,\theta) = h(r) \tag{12}$$

$$\int\int h(x,y)\mathrm{d}x\,\mathrm{d}y = 1 \tag{13}$$

In polar domain, the Gaussian PSF $h(r)$ can be expressed as

$$h(r) = \frac{1}{2\pi\sigma^2} \cdot e^{-\frac{r^2}{2\sigma^2}} \tag{14}$$

The relationship between ZMs for the original image $Z_{p,q}^{(f)}$, the blur image $Z_{p,q}^{(g)}$ and the PSF $Z_{p,q}^{(h)}$ as given in [6] is

$$Z_{p,q}^{(g)} = \sum_{i=0}^{l} Z_{q+2i,q}^{(f)} \sum_{j=0}^{l-i} Z_{2j,0}^{(h)} \sum_{k=i+j}^{l} \sum_{n=i}^{k-j} \binom{q+k}{q+n}\binom{k}{n} c_{l,k}^{q} d_{n,i}^{q} d_{k-n,j}^{0} \tag{15}$$

where c and d are given by

$$c_{l,k}^{q} = (-1)^{l-k} \frac{q+2l+1}{\pi} \frac{(q+l+k)!}{k!(l-k)!(q+k)!}$$

$$d_{i,j}^{q} = \frac{i!(q+i)!\pi}{(i-j)!(q+i+j+1)!} \tag{16}$$

The relationship for the EZM can be obtained by replacing the ZM in Eq. (15) with EZM:

$$EZM_{p,q}^{(g)} = \sum_{i=0}^{l} EZM_{q+2i,q}^{(f)} \sum_{j=0}^{l-i} EZM_{2j,0}^{(h)} \sum_{k=i+j}^{l} \sum_{n=i}^{k-j} \binom{q+k}{q+n} \binom{k}{n} c_{l,k}^{q} d_{n,i}^{q} d_{k-n,j}^{0} \tag{17}$$

where c and d are given in Eq. (16).

4. Formulation of the proposed blur metric using exact Zernike moments

In this section a no-reference blur metric that considers the difference between the edge points of the test image and the re-blurred version of the same image is proposed. This is because the degree of blurring affects the edges. A set of EZM that closely models the HVS perception of blur images is derived. Then, the proposed blur metric which consists of two stages is developed. In the first stage, the weighted EZMs local scores are obtained by combining the EZMs differences and the GM dissimilarities of the edge points between the test image and the re-blurred version of the test image. In the second stage, the means of the weighted EZMs local scores for all the edge points are computed and fed into the SVR to produce a single quality score.

4.1. Selection of EZMs features for Gaussian blur

Both ZMs and EZMs are rotationally invariant. This characteristic is of great advantage to evaluate the edge in the image because their magnitudes are not affected by the edge direction. However, EZMs is chosen in this study because it solves the existence of the numerical errors arising from the computation of ZMs [45]. This improved performance makes it a better NR blur metric than using ZMs, which is shown in the next section.

By substituting Eq. (11) into Eq. (1), EZMs for a Gaussian blur kernel, h, $EZM^{(h)}$ can be expressed as

$$EZM_{p,q}^{(h)} = \int_0^{2\pi} \int_0^1 \frac{1}{2\pi\sigma^2} e^{-\frac{r^2}{2\sigma^2}} R_{p,q}(r) e^{-\hat{j}q\theta} r \, \mathrm{d}r \, \mathrm{d}\theta \tag{18}$$

Now consider a Gaussian blur kernel h, the zero-th order EZMs computed from Eq. (9) becomes

$$EZM_{0,0}^{(h)} = \frac{1}{\pi} \sum_x \sum_y h(x,y) \tag{19}$$

Due to imaging system that is energy-preserving system, $EZM_{0,0}^{(h)} = 1/\pi$. Irrespective of the changes in σ, $EZM_{0,0}^{(h)}$ remains a constant.

By setting $p=2$ and $q=0$, $EZM_{2,0}^{(h)}$ can be expressed in term of the standard deviation of the Gaussian distribution, σ, as given by

$$EZM_{2,0}^{(h)} = -1 + 4\sigma^2 - e^{-\frac{1}{2\sigma^2}}\left(1 + 4\sigma^2\right) \tag{20}$$

A plot of how the value of $EZM_{2,0}^{(h)}$ changes as the degree of blurriness increases is shown in Fig. 1(a). From the figure, it can be seen that as the standard deviation of the Gaussian distribution for the blurring kernel increases, the absolute value of the $EZM_{2,0}^{(h)}$ decreases

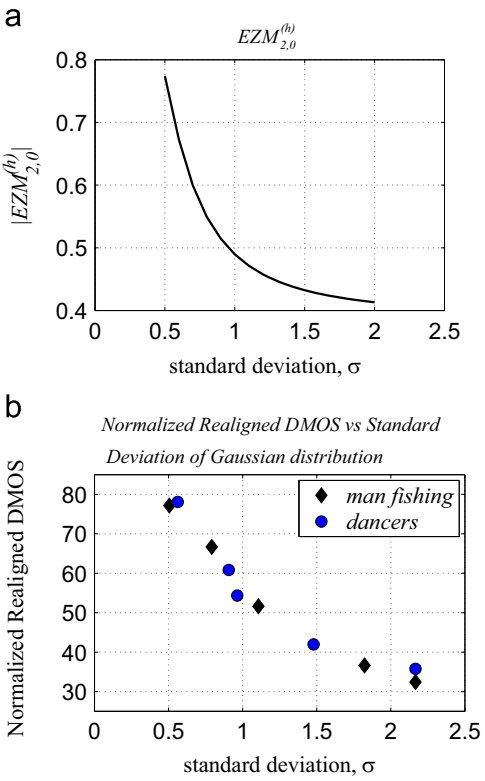

Fig. 1. (a) The absolute value of $EZM_{2,0}^{(h)}$ monotonically decreases as the standard deviation of the Gaussian distribution for the Gaussian blur kernel increases, (b) correlation between human subjective scores and the standard deviation of the Gaussian distribution for Gaussian blur images *Man Fishing* and *Dancers* from LIVE image database.

monotonically. This is in accordance with the correlation between the human subjective score with the degree of blurriness, σ for the LIVE image database [35], as shown in Fig. 1(b). The LIVE image database consists of twenty nine reference images, and for the Gaussian blur images, five different levels of distortion were applied. Twenty four observers evaluated the quality of the images and the ratings were reported in DMOS. Note that the DMOS score has been normalized such that higher score corresponds to sharper image, whereas lower score corresponds to blurrier image.

Since $EZM_{0,0}^{(h)}$ is a constant, and $EZM_{2,0}^{(h)}$ emulates human perception towards images with various degree of Gaussian blur, by setting constraint of $l-i \leq 1$ in Eq. (17), we derive a set of $EZM^{(g)}$ which is only related to $EZM_{0,0}^{(h)}$ and $EZM_{2,0}^{(h)}$:

$$EZM_{2,0}^{(g)} = \left(3EZM_{0,0}^{(f)} + EZM_{2,0}^{(f)}\right) + \pi EZM_{0,0}^{(f)} EZM_{2,0}^{(h)}$$

$$EZM_{3,1}^{(g)} = \left(6EZM_{1,1}^{(f)} + EZM_{3,1}^{(f)}\right) + \pi 2EZM_{1,1}^{(f)} EZM_{2,0}^{(h)}$$

$$EZM_{4,2}^{(g)} = \left(10EZM_{2,2}^{(f)} + EZM_{4,2}^{(f)}\right) + \pi \frac{10}{3} EZM_{2,2}^{(f)} EZM_{2,0}^{(h)}$$

$$EZM_{5,3}^{(g)} = \left(15EZM_{3,3}^{(f)} + EZM_{5,3}^{(f)}\right) + \pi 5EZM_{3,3}^{(f)} EZM_{2,0}^{(h)}$$

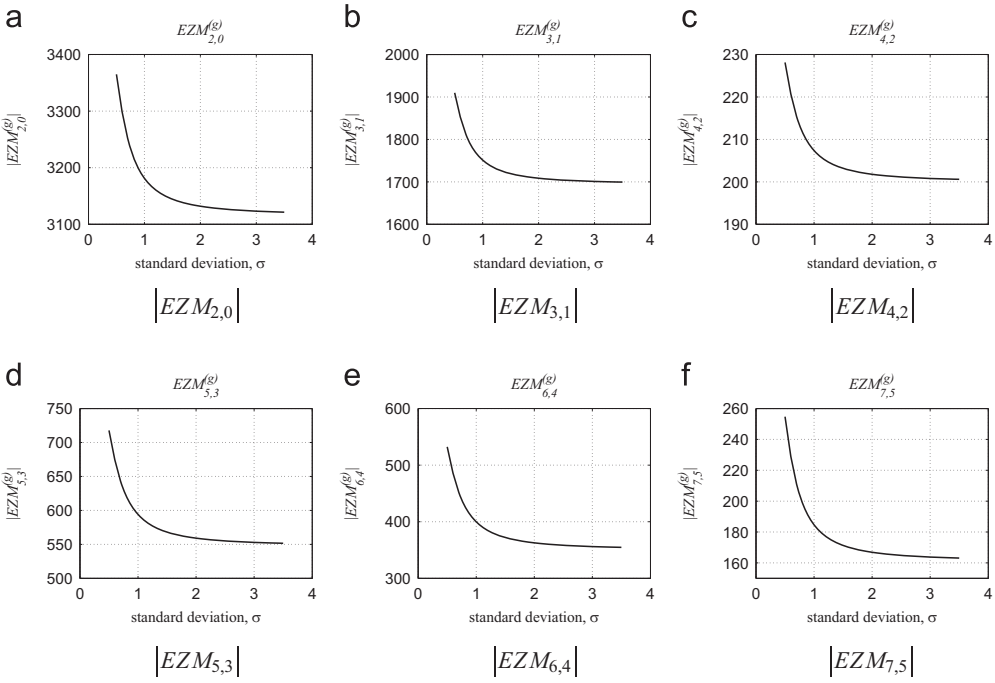

Fig. 2. Six selected EZMs features of 5×5 edge block centered at an edge point and how their magnitudes change with different degrees of Gaussian blur.

$$EZM_{6,4}^{(g)} = \left(21EZM_{4,4}^{(f)} + EZM_{6,4}^{(f)}\right) + \pi 7 EZM_{4,4}^{(f)} EZM_{2,0}^{(h)}$$
$$EZM_{7,5}^{(g)} = \left(28EZM_{5,5}^{(f)} + EZM_{7,5}^{(f)}\right) + \pi \frac{28}{3} EZM_{5,5}^{(f)} EZM_{2,0}^{(h)} \tag{21}$$

Extending the observed relationship of $EZM_{2,0}^{(h)}$ to $EZM_{p,p-2}^{(g)}$, we show in Fig. 2 the results of how these $EZM^{(g)}$ for a 5×5 edge block centered at an edge point vary with the changes in the standard deviation. As the standard deviation of the Gaussian kernel increases (the degree of blurriness increases), the absolute values of these $EZM_{p,p-2}^{(g)}$ decrease monotonically. This is in accordance with the correlation between the human subjective score with the σ for the LIVE image database.

The general equation that monotonically relates $EZM^{(g)}$ with order p and repetition $p-2$ to the degree of blurriness is given by:

$$EZM_{p,q}^{(h)} = \int_0^{2\pi} \int_0^1 \frac{1}{2\pi\sigma^2} e^{-\frac{r^2}{2\sigma^2}} R_{p,q}(r) e^{-\hat{j}q\theta} r \, \mathrm{d}r \, \mathrm{d}\theta \tag{22}$$

It can be seen that the values of $EZM_{p,p-2}^{(g)}$ are only affected by $EZM_{2,0}^{(h)}$ since $EZM_{p-2,p-2}^{(f)}$ and $EZM_{p,p-2}^{(f)}$ remain constant as they are calculated based on the original image. $EZM_{2,0}^{(h)}$ plays a pivotal role in the trend $EZM_{p,p-2}^{(g)}$ takes as the standard deviation of the Gaussian blur kernel varies. It is significant for the trend to display a monotonic line that follows the expected subject scores for Gaussian blur images, as shown in Fig. 1(b). For the rest of the paper, let F_i denotes $EZM_{i+1,i-1}$, $i = 1, 2, \ldots, 6$.

4.2. Proposed blur metric

The proposed EZM based blur metric computation consists of two stages: (1) in the first stage, the local blur score is computed from EZMs (denoted by $F_i, i = 1, 2, \ldots, 6$) and the GM (which is denoted by G), (2) the local blur scores are pooled into a single blur index to quantify the image quality. Superscript t denotes the features calculated for the test image while superscript r denotes the features calculated for the re-blurred version of the test image.

Fig. 3 shows the flowchart of the proposed blur metric. The edge detection algorithm is applied to the test image by convolving the test image with edge operator kernel. Based on the edge strengths, actual edge points are obtained by adaptive thresholding. After the edge map of the test image is constructed, each edge point is used as the center of a 3×3 block. F^t and G^t are calculated for every block centered at the edge point. The test image is re-blurred using a Gaussian blur kernel. F^r and G^r are computed on the re-blurred version of the test image based on the edge points extracted from the test image. This is because the differences are measured at the same location after re-blurring process has been applied to the test image.

For every edge point, the absolute difference of the EZMs, S_{F_i} for $i = 1, 2, \ldots, 6$, and the dissimilarity of the GM, S_G are computed as follow:

$$S_{F_i}(k) = |F_i^t(k) - F_i^r(k)| \tag{23}$$

$$S_G(k) = 1 - \frac{2G^t(k) \cdot G^r(k)}{(G^t(k))^2 + (G^r(k))^2} \tag{24}$$

where $k = 1, 2, \ldots, K$, K is the number of edge point of the test image. An example of how the F_1^t, F_1^r and S_{F_1} using $EZM_{2,0}$ vary as the standard deviation of the Gaussian blur increases is shown

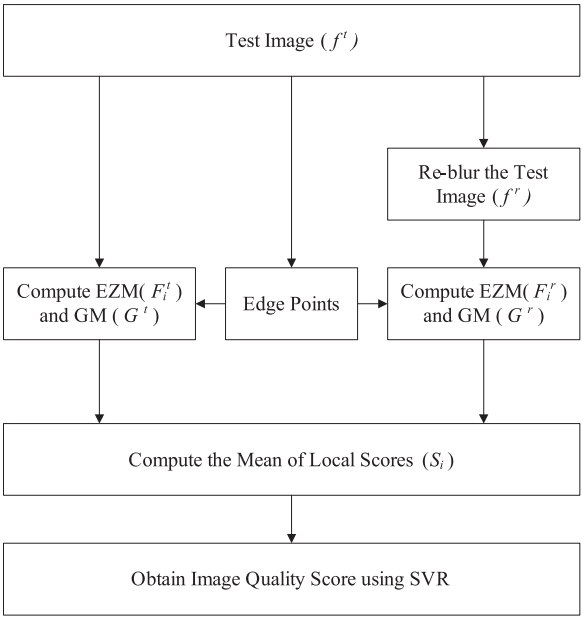

Fig. 3. Flowchart of the proposed blur metric.

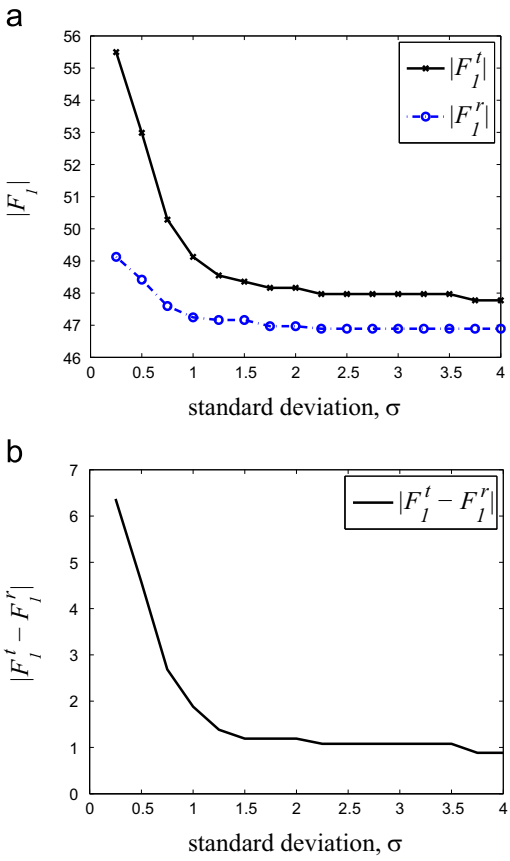

Fig. 4. (a) Both the $|EZM_{2,0}|$ for the edge block $|F_1^t|$ and $|EZM_{2,0}|$ for the re-blurred version of the edge block $|F_1^r|$ decrease as the standard deviation of the Gaussian blur, σ increases. (b) S_{F_1} value is larger when the standard deviation σ is small, and decreases as the σ increases.

in Fig. 4. Only the magnitude is shown because EZMs consists of real and imaginary parts. The local scores, S_{L_i}, for $i = 1, 2, \ldots, 6$ are then computed using

$$S_{L_i}(k) = [S_G(k)]^{\alpha} \cdot \left[S_{F_i}(k)\right]^{\beta} \tag{25}$$

where α and β are parameters used to adjust the relative importance of EZM and GM features. For simplicity, we set $\alpha = \beta = 1$ in this paper. Thus, $S_{L_i}(k) = S_G(k) \cdot S_{F_i}(k)$. In other word, the local score is calculated from EZMs weighted by GM. The overall score of the test image is computed by taking the mean values of the local scores.

$$S_i = \frac{\sum_{k=1}^{K} S_{L_i}(k)}{K} \tag{26}$$

The $S_1 - S_6$ values for the Gaussian blur images from LIVE image database with respect to the DMOS score are shown in Fig. 5. Table 1 shows the three different level of Gaussian blur degradations of image *Parrots* from the LIVE image database [35] and their DMOS and $S_1 - S_6$ values. From the table, it can be seen that the values $S_1 - S_6$ decrease as the σ and DMOS increase.

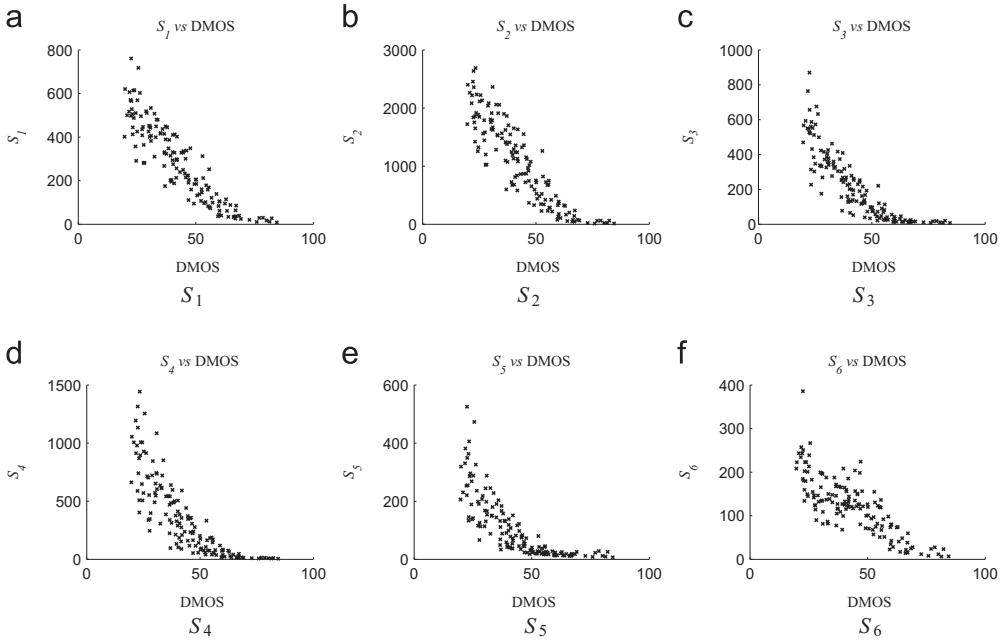

Fig. 5. S_1–S_6 values for the Gaussian blur images from LIVE image database with respect to the DMOS score.

Table 1
Example of *Parrots* image from LIVE image database with different level of Gaussian blur degradation and their $S_1 - S_6$.

	S_1	S_2	S_3	S_4	S_5	S_6
 σ = 0.7916 DMOS = 23.7478	583.32	2448.75	390.32	637.46	156.04	302.09
 σ = 2.1667 DMOS = 52.1681	187.39	653.53	60.22	113.86	30.07	142.62
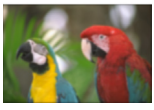 σ = 4.0000 DMOS = 69.2956	66.83	123.06	15.90	27.51	16.07	32.23

Since images are naturally multiscale and blurring affects image structure across scales, we extract the EZM features at two scales – original image scale and at a reduced resolution (downsampled by 2). Thus, a total of 12 features – $S_1 - S_{12}$ are used for the quality assessment.

4.3. BIQA prediction model learning

The proposed EZMs based blur metric (EZMBM) score is obtained by mapping the feature space consisted of twelve features $S_1 - S_{12}$ to the quality score by using support vector machine (SVM) regressor (SVR). ε-SVR is employed in this paper for the mapping. For a set of given training data $(x_1, y_1), (x_2, y_2), \ldots, (x_k, y_k)$, where $x_i, i = 1, 2, \ldots, k$ is the feature vector and y_i is the DMOS score, we aim to find a function to predict the score from the input feature vector: $f(x) = \langle w, x \rangle + b$, where $\langle \cdot, \cdot \rangle$ denotes the inner product, w is the weight vector and b is the bias parameter. By introducing the slack variables ξ_i and ξ_i^*, w and b can be computed by solving the following optimization problem:

$$\begin{aligned} &\text{minimize} \frac{1}{2} \| w \|^2 + C \sum_{i=1}^{k} \left(\xi_i + \xi_i^* \right) \\ &\text{subject to} \begin{cases} \langle w, x_i \rangle - (y_i - b) \leq \varepsilon + \xi_i \\ (y_i - b) - \langle w, x_i \rangle \leq \varepsilon + \xi_i^* \\ \xi_i, \xi_i^* \geq 0 \end{cases} \end{aligned} \tag{27}$$

where C is a constant parameter to control the amount of influence of the error and $\frac{1}{2} \| w \|^2$ term controls the complexity of the regression function. The minimizer of Eq. (27) is given by: $w = \sum_{i=1}^{k} t_i x_i$, where t_i is the combination coefficient. We first map the input feature vector into a high dimensional feature space $\Phi(x)$, and then learn the regression function:

$$\begin{aligned} f(x) &= \left\langle \sum_{i=1}^{k} t_i \Phi(x_i), \Phi(x) \right\rangle + b \\ &= \sum_{i=1}^{k} t_i \langle \Phi(x_i), \Phi(x) \rangle + b \end{aligned} \tag{28}$$

The inner product $\langle \Phi(x_i), \Phi(x) \rangle$ can be written as a kernel function $K(x_i, x)$, and Eq. (28) becomes

$$f(x) = \sum_{i=1}^{k} t_i K(x_i, x) + b \tag{29}$$

In this paper, LIBSVM package [5] is utilized to implement the $\varepsilon-$ SVR with a radial basis function (RBF) $K(x_i, x) = exp\left(-\gamma(|x_i - x|)^2\right)$ is used as the kernel function, where γ is the precision parameter.

5. Performance evaluation

In this section, first, the databases and methods used for the comparisons are described. Next, the implementation details are given, followed by a study on the effect of using different sizes of window for the EZM calculation. The proposed blur metric is then compared with other existing

FR and NR blur metrics using LIVE, TID2008 and CSIQ image databases. An experiment on the database dependency is performed to check the robustness of the proposed blur metric.

5.1. Databases and methods for comparison

We use Gaussian blur images from the LIVE [35], TID2008 [32] and CSIQ [19] image databases to test the performance of the EZMBM and other existing blur metrics used in the study. DMOS are provided by LIVE and CSIQ databases, whereas MOS is provided by TID2008 database. The LIVE database consists of 145 Gaussian blur distorted images, generated from 29 reference color images by applying 5 different levels of distortion. The CSIQ and TID2008 databases consist of 30 and 25 color reference images, respectively. 5 levels of Gaussian blur distortion are applied to the CSIQ reference images whereas 4 levels of Gaussian blur distortion are applied to the TID2008 reference images. A summary of these three databases is shown in Table 2.

Pearson's correlation coefficient (CC) and Spearman's rank ordered correlation coefficient (SROCC) between the predicted score and DMOS are employed to evaluate the performance of the NR blur metrics. CC indicates the prediction accuracy after the linear/non-linear regression, whereas SROCC predicts the monotonicity. SROCC only operates on the rank of the data points, and thus not affected by linear/non-linear regression. The logistic fitting function used for the non-linear regression is given by [36]

$$f(x) = \beta_1 \left(\frac{1}{2} - \frac{1}{1 + e^{\beta_2 (x - \beta_3)}} \right) + \beta_4 x + \beta_5 \tag{30}$$

where $\beta_i, i = 1, 2, \ldots, 5$, are the model parameters, $f(x)$ is the predicted DMOS and x is the metric to be fitted in. A value closes to 1 for CC and SROCC indicates good performance for the NR blur metric.

5.2. Implementation details

Since the range of DMOS/MOS for LIVE database, CSIQ database and TID2008 are different, we rescale the DMOS of CSIQ and the MOS of TID2008 databases to the range of the DMOS for LIVE database. Since the DMOS for LIVE is $[0, 100]$ (where 0 is the best quality and 100 is the worst quality), and the proposed EZMBM has the range of $[0, 1]$ (0 is the worst quality and 1 is the best quality), we can easily relate them by $EZMBM = (100 - DMOS)/100$.

In order to calculate the features for a test image for the proposed blur metric, the test image needs to be reblurred with a σ of the Gaussian filter. We set σ to 1.0 as it is used just to create a relative blurred image. The window of this reblurring filter is set to 5×5. To investigate the size of the EZM local window, we set the window size to $3 \times 3, 5 \times 5, 7 \times 7$ and 9×9, and compute

Table 2
Test databases for blur image comparison.

Database	Source images	Distorted images	Image type	Observers
LIVE [35]	29	145	Color	161
CSIQ [19]	30	150	Color	35
TID2008 [32]	25	100	Color	838

Table 3
Performance of EZMBM on LIVE image database Gaussian blur images for different window sizes.

Window size	CC
3×3	0.9625
5×5	0.9591
7×7	0.9524
9×9	0.9522

the CC values on the *LIVE* image database. The results are shown in Table 3. We can see that the EZM local window size of 3×3 leads to higher CC. As the window size increases, the CC values decrease. In all the following experiments, we set the EZM local window size to be 3×3.

When using the LIBSVM package's SVR [5] to learn the regression model, we conduct a cross validation experiment to choose the values of (C, γ). We divide each of the database into two randomly chosen subset, where 80% is for training and the remaining 20% is for testing. This is to ensure no overlap between the training and testing sets occurs. The model learned from the training set is applied and examined on the testing set. This random training-testing procedure is repeated 1000 times and the median results of the performance across these 1000 iteration is reported in order to eliminate performance bias. The (C, γ) values delivering the median results are chosen as the model parameters. The optimal (C, γ) were found to be $(128, 0.25)$, $(4, 32)$ and $(1024, 1)$ on the LIVE, TID2008 and CSIQ databases, respectively.

5.3. Comparison performance with existing blur metrics using LIVE, TID2008 and CSIQ databases

The proposed EZMBM is compared with some of the state-of-the-art NR algorithms (JNB metric [13], CPBD [29], Li et al. [20], BLIINDS-II [33], DIIVINE [27], BRISQUE [26] and Xue et al. M_3 [47]) and another one is the earlier, but well-received, GPVM [9], and also the blur metric but using ZM known as ZMBM. The proposed algorithm is written in MATLAB and all the performance evaluations are run in MATLAB. Implementations of all these metrics are available at [14,2]. In addition to that, we also tabulate the performance of five FR metrics: peak-signal-to-noise ratio (PSNR), structural similarity index (SSIM) [42], multi-scale structural similarity index (MS-SSIM) [44] and low-level feature similarity index (FSIM and FSIMc) [51]. Although PSNR is a poor measure of perceptual quality, it is still often used as benchmark for IQA. FSIM operates on luminance values only while FSIMc includes color information in its quality index.

Table 4 lists the CC and SROCC results of the EZMBM and other existing FR/NR blur metrics on the LIVE database for Gaussian blur images. Note that the reported results for EZMBM are the median values across 1000 random train-test procedure. From the experimental results in the table, it can be seen that the proposed EZMBM outperforms other existing NR blur metrics for SROCC for the LIVE database. It also shows the superiority of EZM as features as compared to using ZM for the blur metric. As for the highest value of the CC among the NR blur metrics, it shows that EZMBM correlate much more consistently with the subjective evaluation that other existing NR blur metrics. For the comparison with existing FR blur metrics, only the FSIM and its variant, FSIMc, fare better than EZMBM.

Table 4
Performance comparison of FR blur metrics on LIVE database.

Quality Metric	Type	LIVE	
		CC	SROCC
PSNR	FR	0.7993	0.7734
SSIM [42]	FR	0.8740	0.8942
MS-SSIM [44]	FR	0.9485	0.9516
FSIM [51]	FR	0.9722	0.9710
FSIMc [51]	FR	0.9723	0.9711
Li et al. [20]	NR	0.9329	0.9252
JNBM [13]	NR	0.7431	0.7521
CPBD [29]	NR	0.9033	0.9053
GPVM [9]	NR	0.8800	0.8750
BLIIND-II [33]	NR	0.8994	0.8912
DIIVINE [27]	NR	0.9370	0.9373
BRISQUE [26]	NR	0.9506	0.9511
M_3 [47]	NR	0.9221	0.8759
ZMBM	NR	0.9635	0.9588
EZMBM	NR	0.9659	0.9625

Table 5
Performance comparison of NR blur metrics on TID2008 and CSIQ databases.

Quality Metric	TID2008		CSIQ	
	CC	SROCC	CC	SROCC
BLIIND-II	0.8982	0.9219	0.9003	0.9082
DIIVINE	0.8930	0.9038	0.8697	0.9010
BRISQUE	0.9357	0.9391	0.9085	0.9356
M_3	0.9369	0.9406	0.9243	0.9457
EZMBM	0.9323	0.9409	0.9285	0.9333

The performance comparison of the EZMBM with existing NR blur metrics on TID2008 and CSIQ databases are listed in Table 5. It can be seen that the EZMBM has the highest correlation with the human subjective scores for the TID2008 database and the performance for the CSIQ database is competitive as compared to the other NR blur metrics.

5.4. Database dependency test

In the experiments in Section 5.3, the BIQA model is learned from and tested on the same database. In order to show the robustness of the proposed EZMBM, it is necessary to test the performance of the BIQA model learned from one database and tested on another database. We adopted a process presented in [26] to test the performance of the proposed method. First, we train the EZMBM on LIVE database, and test it on the TID2008 and CSIQ databases. Then, we train it on the TID2008 database, and test it on LIVE and CSIQ databases. Lastly, we train it on

Table 6
SROCC performance comparison for database dependency test.

Database for training	Database for testing	DIVINE	BLIINDS2	BRISQUE	M_3	EZMBM
LIVE	CSIQ	0.8571	0.8878	0.8993	0.9108	0.8986
LIVE	TID2008	0.8599	0.9056	0.9050	0.9204	0.8393
TID2008	LIVE	0.8658	0.9389	0.9228	0.9336	0.9200
TID2008	CSIQ	0.8481	0.8747	0.8665	0.8393	0.8672
CSIQ	LIVE	0.8475	0.9365	0.9311	0.9459	0.9367
CSIQ	TID2008	0.8223	0.8005	0.8986	0.9051	0.8409

CSIQ database, and test it on the LIVE and TID2008 databases. This training-testing procedure is applied to the other 3 existing NR blur metrics for comparison. The results are tabulated in Table 6. The EZMBM performance is comparable to the NR existing blur metrics.

6. Conclusion

In this paper, we present a novel NR blur metric using exact Zernike moment and gradient magnitude for digital images. We derive and show the proposed set of EZMs closely model the human evaluation score for digital images with various blur degrees. The rotation invariance property of exact Zernike moments gives an advantage that the features will not be affected by the direction of the edges. We use six of these EZMs, together with GM as weight to encode contrast information for the proposed EZMBM. The EZMBM is compared with seven NR blur metrics and also the ZMBM that used ZM as features. Experimental results show that the proposed blur metric performs better than other existing NR blur metrics, achieving Pearson correlation coefficient (CC) and Spearman's ranked-order correlation coefficient (SROCC) of 0.9659 and 0.9625 respectively for the LIVE image database. This shows that the proposed EZMBM correlates well with human evaluation on digital images with various blur degrees.

Acknowledgment

This work was supported by the Engineering Faculty of the University of Malaya under Grant No. UM.C/HIR/MOHE/ENG/42.

References

[1] G. Amayeh, G. Bebis, A. Erol, M. Nicolescu, Peg-free hand shape verification using high order Zernike moments, in: 2006 Conference on Computer Vision and Pattern Recognition Workshop, CVPRW'06, 2006, p. 40.
[2] D.Q. Bao, Gpvm image blur metric matlab code [online], ⟨http://www.mathworks.com/matlabcentral/fileexchange/24676-image-blur-metric⟩, 2014.
[3] C. Batten, Autofocusing and astigmatism correction in the scanning electron microscope (Ph.D. thesis), Faculty of the Department of Engineering, University of Cambridge, UK, 2000.
[4] J. Caviedes, F. Oberti, A new sharpness metric based on local kurtosis, edge and energy information, Signal Process.: Image Commun. 19 (2004) 147–161.
[5] C.C. Chang, C.J. Lin, Libsvm: A Library for Support Vector Machines, Software, 2001.
[6] B. Chen, H. Shu, H. Zhang, G. Coatrieux, L. Luo, J.L. Coatrieux, Combined invariants to similarity transformation and to blur using orthogonal Zernike moments, IEEE Trans. Image Process. 20 (2011) 345–360.

[7] N. Chern, P. Neow, M. Ang Jr., Practical issues in pixel-based autofocusing for machine vision, in: IEEE International Conference on Robotics and Automation, 2001, Proceedings 2001 ICRA, IEEE, vol. 3, 2001, pp. 2791–2796.
[8] C.W. Chong, R. Mukundan, R. Paramesran, An efficient algorithm for fast computation of Zernike moments, in: Proceedings of the 6th Joint Conference on Information Science, JCIS'02, Research Triangle Park, NC, 2002, pp. 785–788.
[9] F. Crete, T. Dolmiere, P. Ladret, M. Nicolas, The blur effect: perception and estimation with a new no-reference perceptual blur metric, Hum. Vis. Electron. Imaging XII 6492 (2007) 11.
[10] S. Dudani, K. Breeding, R. McGhee, Aircraft identification by moment invariants, IEEE Trans. Comput. 100 (1977) 39–46.
[11] S. Erasmus, K. Smith, An automatic focusing and astigmatism correction system for the sem and ctem, J. Microsc. 127 (1982) 185–199.
[12] R. Ferzli, L. Karam, No-reference objective wavelet based noise immune image sharpness metric, in: IEEE International Conference on Image Processing, vol. 1, 2005, pp. 405–408.
[13] R. Ferzli, L. Karam, A no-reference objective image sharpness metric based on the notion of just noticeable blur (jnb), IEEE Trans. Image Process. 18 (2009) 717–728.
[14] R. Ferzli, L. Karam, Ivu lab [online], ⟨http://ivulab.asu.edu/⟩, 2014.
[15] L. Firestone, K. Cook, K. Culp, N. Talsania, K. Preston Jr, Comparison of autofocus methods for automated microscopy, Cytometry 12 (1991) 195–206.
[16] S. Ghosal, R. Mehrotra, Orthogonal moment operators for subpixel edge detection, Pattern Recognit. 26 (1993) 295–306.
[17] M.K. Hu, Visual pattern recognition by moment invariants, IRE Trans. Inf. Theory 8 (1962) 179–187.
[18] Z. Iscan, Z. Dokur, T. Ölmez, Tumor detection by using Zernike moments on segmented magnetic resonance brain images, Expert Syst. Appl. 37 (2010) 2540–2549.
[19] E. Larson, D.M. Chandler, Categorical image quality (csiq) database 2009 [online], ⟨http://vision.okstate.edu/csiq⟩, 2009.
[20] C. Li, W. Yuan, A. Bovik, X. Wu, No-reference blur index using blur comparisons, Electron. Lett. 47 (2011) 962–963.
[21] C.L. Lim, B. Honarvar, K.H. Thung, R. Paramesran, Fast computation of exact Zernike moments using cascaded digital filters, Inf. Sci. 181 (2011) 3638–3651.
[22] W. Liyun, L. Hefei, Z. Fuhao, L. Zhengding, W. Zhendi, Spermatogonium image recognition using Zernike moments, Comput. Methods Progr. Biomed. 95 (2009) 10–22.
[23] R.A. Manap, L. Shao, Non-distortion-specific no-reference image quality assessment: a survey, Inf. Sci. 301 (2015) 141–160.
[24] X. Marichal, W. Ma, H. Zhang, Blur determination in the compressed domain using dct information, in: Proceedings of 1999 International Conference on Image Processing, 1999, ICIP 99, IEEE, vol. 2, 1999, pp. 386–390.
[25] P. Marziliano, F. Dufaux, S. Winkler, T. Ebrahimi, Perceptual blur and ringing metrics: application to jpeg2000, Signal Process.: Image Commun. 19 (2004) 163–172.
[26] A. Mittal, A.K. Moorthy, A.C. Bovik, No-reference image quality assessment in the spatial domain, IEEE Trans. Image Process. 21 (2012) 4695–4708.
[27] A.K. Moorthy, A.C. Bovik, Blind image quality assessment: from natural scene statistics to perceptual quality, IEEE Trans. Image Process. 20 (2011) 3350–3364.
[28] R. Mukundan, S. Ong, P.A. Lee, Image analysis by Tchebichef moments, IEEE Trans. Image Process. 10 (2001) 1357–1364.
[29] N. Narvekar, L. Karam, A no-reference image blur metric based on the cumulative probability of blur detection (cpbd), IEEE Trans. Image Process. 20 (2011) 2678–2683.
[30] M. Novotni, R. Klein, 3d Zernike descriptors for content based shape retrieval, in: Proceedings of the Eighth ACM Symposium on Solid Modeling and Applications, ACM, 2003, pp. 216–225.
[31] G. Paschos, I. Radev, N. Prabakar, Image content-based retrieval using chromaticity moments, IEEE Trans. Knowl. Data Eng. 15 (2003) 1069–1072.
[32] N. Ponomarenko, K. Egiazarian, Tampere image database 2008 tid2008 [online], ⟨http://www.ponomarenko.info/tid2008.htm⟩, 2008.
[33] M.A. Saad, A.C. Bovik, C. Charrier, Blind image quality assessment: a natural scene statistics approach in the dct domain, IEEE Trans. Image Process. 21 (2012) 3339–3352.
[34] D. Shaked, I. Tastl, Sharpness measure: Towards automatic image enhancement, in: IEEE International Conference on Image Processing, ICIP 2005, vol. 1, IEEE, 2005, pp. I–937.

[35] H. Sheikh, Z. Wang, L. Cormack, A. Bovik, Live image quality assessment database release 2 [online], ⟨http://live.ece.utexas.edu/research/quality/subjective.htm⟩, 2005.
[36] H.R. Sheikh, M.F. Sabir, A.C. Bovik, A statistical evaluation of recent full reference image quality assessment algorithms, IEEE Trans. Image Process. 15 (2006) 3440–3451.
[37] J. Shen, Q. Li, G. Erlebacher, Hybrid no-reference natural image quality assessment of noisy, blurry, jpeg2000, and jpeg images, IEEE Trans. Image Process. 20 (2011) 2089–2098.
[38] M.R. Teague, Image analysis via the general theory of moments, J. Opt. Soc. Am. 70 (1980) 920–930.
[39] C. Teh, R. Chin, On image analysis by the methods of moments, IEEE Trans. Pattern Anal. Mach. Intell. 10 (1988) 496–513.
[40] K.H. Thung, R. Paramesran, C.L. Lim, Content-based image quality metric using similarity measure of moment vectors, Pattern Recognit. 45 (2012) 2193–2204.
[41] H. Tong, M. Li, H. Zhang, C. Zhang, Blur detection for digital images using wavelet transform, in: 2004 IEEE International Conference on Multimedia and Expo, ICME'04, vol. 1, IEEE, 2004, pp. 17–20.
[42] Z. Wang, A. Bovik, H. Sheikh, E. Simoncelli, Image quality assessment: from error visibility to structural similarity, IEEE Trans. Image Process. 13 (2004) 600–612.
[43] Z. Wang, A.C. Bovik, Modern image quality assessment, Synth. Lect. Image Video Multimed. Process. 2 (2006) 1–156.
[44] Z. Wang, E.P. Simoncelli, A.C. Bovik, Multiscale structural similarity for image quality assessment, in: Conference Record of the Thirty-Seventh Asilomar Conference on Signals, Systems and Computers, vol. 2, IEEE, 2004, pp. 1398–1402.
[45] C. Wee, R. Paramesran, On the computational aspects of Zernike moments, Image Vis. Comput. 25 (2007) 967–980.
[46] C.Y. Wee, R. Paramesran, R. Mukundan, X. Jiang, Image quality assessment by discrete orthogonal moments, Pattern Recognit. 43 (2010) 4055–4068.
[47] W. Xue, X. Mou, L. Zhang, A.C. Bovik, X. Feng, Blind image quality assessment using joint statistics of gradient magnitude and Laplacian features, IEEE Trans. Image Process. 23 (2014) 4850–4862.
[48] P. Yap, R. Paramesran, Content-based image retrieval using Legendre chromaticity distribution moments, in: IEE Proceedings – Vision, Image and Signal Processing, vol. 153, IET, 2006, pp. 17–24.
[49] P. Yap, P. Raveendran, Image focus measure based on Chebyshev moments, in: IEE Proceedings – Vision, Image and Signal Processing, vol. 151, IET, 2004, pp. 128–136.
[50] P.T. Yap, R. Paramesran, S.H. Ong, Image analysis by Krawtchouk moments, IEEE Trans. Image Process. 12 (2003) 1367–1377.
[51] L. Zhang, D. Zhang, X. Mou, Fsim: a feature similarity index for image quality assessment, IEEE Trans. Image Process. 20 (2011) 2378–2386.
[52] N. Zhang, A. Vladar, M. Postek, B. Larrabee, A kurtosis-based statistical measure for two-dimensional processes and its application to image sharpness, Proc. Sect. Phys. Eng. Sci. Am. Stat. Soc. (2003) 4730–4736.